Scientia Iranica, Vol. 14, No. 3, pp 193 204

SCIENTIA IRANICA

Mixed Shear-Flexural (VM) Hinge Element and Its Applications

M.T. Kazemi* **and S. Erfani**[1]

In the present paper, a mixed, shear-flexural (VM) hinge element, with zero or nonzero length, for using in frames, has been introduced, where shear-flexural interaction has been considered. The element has the capability of modeling flexural yielding, shear yielding and their interaction in frames, subjected to all kinds of monotonic or cyclic loadings. The inelastic shear and flexural deformations and tangential stiffnesses are considered by using the multi-surfaces approach with dissimilar yield surfaces and by a stiffness matrix with nonzero off-diagonal components. A new kinematics hardening rule and, also, a new non-associated flow rule are introduced. The mixed hinge element can be used in the arbitrary location of beam-column elements, where shear effect is significant. The model is examined for some link beams in eccentrically braced steel frames (EBFs) and it is shown that the analytical and experimental results have excellent agreement. Some reduced web section beams are investigated, too. It is shown that the mixed hinge results are in good agreement with the finite element results.

INTRODUCTION

Inelastic analysis and design of structures have made great progress, due to the rapid development of computer hardware and software in recent decades [1-4]. The common approach for representing inelastic behavior in a beam-column element is to adopt inelastic hinge formation. A generalized plastic hinge, with zero length, accounting for the interaction of axial, torsional and biaxial bending moments, based on the multi-surfaces plasticity concept, was presented by Powell and Chen [5]. Krenk et al. [6], by using a piecewise linearized yield surface and a linear kinematic hardening rule for concentrated hinges, developed a formulation for displacement discontinuities with extension and rotation components. A method for modeling the members with yielding under combined flexure and axial forces in steel frames subjected to earthquake ground motion was presented by Kim and Engelhardt [7]. This method had the capability of modeling plastic axial deformation and changes in axial stiffness, based on isotropic and kinematic strain-hardening, defined in axial-flexural space. The multi-surface yield concept was used in all the works mentioned above. Liew et al. [8-10] used the two-surface plasticity concept for considering the inelastic interaction between axial force and bending moment, too. The effect of shear force was ignored in all of the above research. El-Tawil and Deierlein [11] investigated two-surface plasticity models in stress-resultant space, based on fiber element analysis. Their research was conducted in an axial force-flexural moment space and the shear force effect was ignored, too, since the fiber element approach is based on a uniaxial stress-strain relationship and the shear force effect is not considered in this approach.

In some cases, shear yielding or combined shear-flexural yielding is the governing behavioral mode. For steel beam sections, plastic moment capacity and flexural rigidity are affected by shear force [1]. Ricles and Popov [12] developed a formulation for modeling links in eccentrically braced steel frames (EBFs), based on the multi-surface plasticity concept. The link beam has a nonlinear hinge at each end. Each hinge consists of uncoupled shear and flexural nonlinear subhinges. Flexural-shear interaction is an important issue in short concrete beams and columns, too. Ricles et al. [13] presented a stress resultant plasticity-based formulation with shear failure criteria and post-shear failure effects, for modeling the response of nonductile reinforced concrete bridge columns subjected to biaxial seismic loading. Kinematic strain hardening and the degradation of elastic unloading stiffness under a cyclic

*. *Corresponding Author, Department of Civil Engineering, Sharif University of Technology, P.O. Box: 11155-9313, Tehran, I.R. Iran.*

1. *Department of Civil Engineering, Sharif University of Technology, P.O. Box: 11155-9313, Tehran, I.R. Iran.*

load reversal for both shear and flexural effects, were accounted for by using an uncoupled shear-flexural hinge approach. A finite element method could also be used for modeling shear-flexural inelastic zones. In frame analysis, using this method for the modeling of inelastic zones takes too much time and is not applicable, practically. Saritas and Filippou [14] investigated the shear-flexural interaction in link beams by using a displacement field, based on Timoshinko's theory and the integration of biaxial stress-strain relations over several control sections along the beams. Each control section subdivided into several layers. This is a general method for considering the axial, shear and flexural interaction in frames. Although the predicted behavior, by using this method, shows good accuracy, because of the need for integration at several points, it takes too much time, the same as in the finite element method.

In the present paper, a mixed VM hinge element, with zero or nonzero length, for using in frames, has been introduced, where shear-flexural interaction has been considered. The mixed hinge element has the capability of modeling flexural yielding, shear yielding, as well as combined shear-flexural yielding. The multi surface concept, with dissimilar yield surfaces and off diagonal components in flexibility matrixes, is used. Elastic and inelastic shear distortion and flexural rotation are considered. The applicability of the proposed mixed hinge element, for link beams in Eccentrically Braced Frames (EBFs) and reduced web section beams in shear-yielding moment-resistant steel frames, is investigated.

DESCRIPTION OF MIXED HINGE ELEMENT

The introduced mixed hinge element includes one inner inelastic combined shear-flexural subhinge with zero length and two rigid parts with zero or nonzero lengths on two sides. Geometrical presentation of this element has been shown in Figure 1, where i and j are the outer nodes and h is the inner subhinge. The inner subhinge has an arbitrary location. The lengths of the two rigid parts are L_i and L_j, and $L = L_i + L_j$ is the total length of the element. The inelastic zones in the frames could be modeled by this element. The properties of the mixed hinge element are defined, such that the relative deformations between the two ends should be equal to the relative deformations between the two ends of the inelastic zone, in real condition. The hinge element will be more representative of the inelastic zone if one takes L as being equal to the length of the inelastic zone.

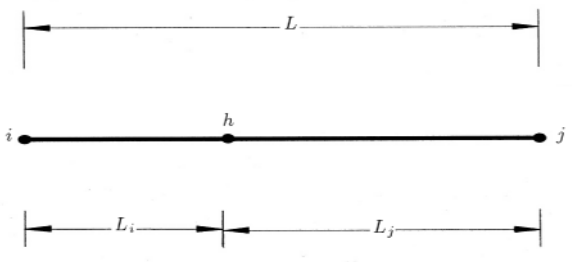

Figure 1. Configurations of the mixed hinge element with a combined flexural-shear subhinge at h.

ELEMENT'S STIFFNESS MATRIX

The mixed hinge element has two end nodes and, in a two-dimensional space, has six degrees of freedom. For definition of these degrees of freedom, a local coordinate system dependent on the element is used. If the element's end forces and displacements are described as $\mathbf{P}$ and $\mathbf{U}$, respectively, it can be written, as follows:

$$\mathbf{P} = \begin{bmatrix} \mathbf{P}_i & \mathbf{P}_j \end{bmatrix}^T, \tag{1}$$

$$\mathbf{U} = \begin{bmatrix} \mathbf{U}_i & \mathbf{U}_j \end{bmatrix}^T, \tag{2}$$

where, $\mathbf{P}_i$, $\mathbf{P}_j$, $\mathbf{U}_i$ and $\mathbf{U}_j$ are nodal forces and displacements at i and j, respectively (see Figure 2). If the element's internal forces and deformations in the inner subhinge node are shown as $\mathbf{P}_h$ and $\mathbf{U}_h$, respectively (see Figure 3), then, one could write:

$$\mathbf{P} = \mathbf{A}\mathbf{P}_h, \tag{3}$$

$$\mathbf{U}_h = \mathbf{A}^T U, \tag{4}$$

where, $\mathbf{A}$ is the transformation matrix and its components are dependent on lengths of rigid parts of the element. It is assumed that no loads and masses are assigned to the subhinge and to the rigid parts, except at the end nodes. It is noted that the deformations are assumed to be small and, then, the initial configuration

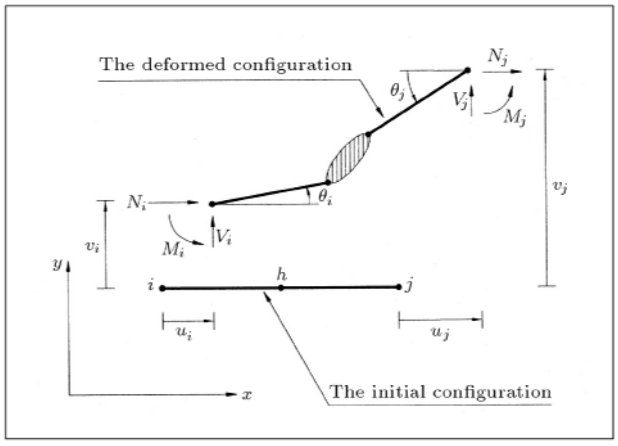

Figure 2. The mixed hinge element's end forces and displacements.

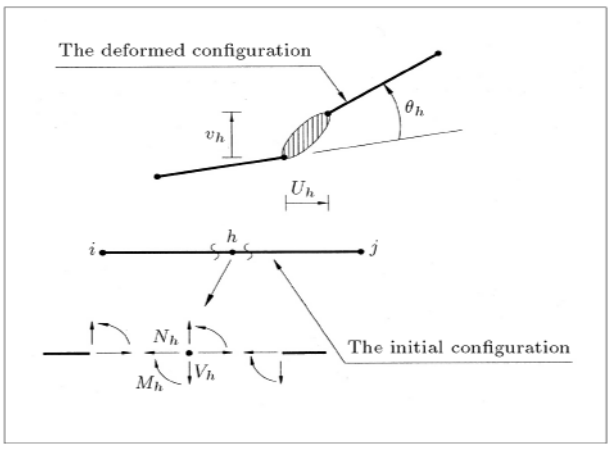

Figure 3. The mixed hinge element's internal forces and deformations.

is used for equilibrium and compatibility considerations. Figure 3 presents the initial and deformed configuration of the mixed hinge element.

If the rates of forces and deformations in the element's inner subhinge are shown as $\dot{\mathbf{P}}_h$ and $\dot{\mathbf{U}}_h$, respectively, then, one could write:

$$\dot{\mathbf{P}}_h = \mathbf{K}_h \dot{\mathbf{U}}_h, \tag{5}$$

$$\dot{\mathbf{U}}_h = \mathbf{F}_h \dot{\mathbf{P}}_h, \tag{6}$$

where, $\mathbf{K}_h$ and $\mathbf{F}_h$ are the tangential stiffness and flexibility matrixes of the subhinge, respectively. Since all of the degrees of freedom in the inner subhinge are independent of each other, both $\mathbf{K}_h$ and $\mathbf{F}_h$ are invertible and inverse to each other.

From Equations 3 to 5, it can be resulted:

$$\dot{\mathbf{P}} = \mathbf{A}\dot{\mathbf{P}}_h = \mathbf{A}\mathbf{K}_h\dot{\mathbf{U}}_h = \mathbf{A}\mathbf{K}_h\mathbf{A}^T\dot{\mathbf{U}}, \tag{7}$$

where, $\dot{\mathbf{P}}$ and $\dot{\mathbf{U}}$ are the element's rate of forces and deformations, respectively. Therefore, for the mixed hinge element stiffness, one could reach:

$$\mathbf{K} = \mathbf{A}\mathbf{K}_h\mathbf{A}^T = \mathbf{A}\mathbf{F}_h^{-1}\mathbf{A}^T, \tag{8}$$

where, $\mathbf{K}$ is the element's stiffness matrix and so:

$$\dot{\mathbf{P}} = \mathbf{K}\dot{\mathbf{U}}. \tag{9}$$

INNER SUBHINGE STIFFNESS AND LOADING-UNLOADING CRITERIA

The components of elastic-plastic tangential stiffness or flexibility matrixes may depend on applied loads or deformations and loading history. The present paper focuses on shear-flexural interaction and ignores the effects of axial force in nonlinear formulation. Thus, the components corresponding to the axial deformation in the stiffness or flexibility matrix remain elastic and constant. By assuming rate independency, in a two dimensional space, Equation 5 can be written as:

$$\begin{Bmatrix} \dot{N}_h \\ \dot{V}_h \\ \dot{M}_h \end{Bmatrix} = \begin{bmatrix} \frac{dN_h}{du_h} & 0 & 0 \\ 0 & \frac{\partial V_h}{\partial \nu_h} & \frac{\partial V_h}{\partial \theta_h} \\ 0 & \frac{\partial M_h}{\partial \nu_h} & \frac{\partial M_h}{\partial \theta_h} \end{bmatrix} \begin{Bmatrix} \dot{u}_h \\ \dot{\nu}_h \\ \dot{\theta}_h \end{Bmatrix}. \tag{10}$$

The components of the tangential stiffness matrix, $\mathbf{K}_h$, are not defined directly. By calculating the inner subhinge's tangential flexibility matrix, $\mathbf{F}_h$, and then inversing it, the tangential stiffness matrix, $\mathbf{K}_h$, is obtained. For small deformation, $\mathbf{F}_h$ can be decomposed as:

$$\mathbf{F}_h = \mathbf{F}_h^e + \mathbf{F}_h^p, \tag{11}$$

where, $\mathbf{F}_h^e$ and $\mathbf{F}_h^p$ are the inner subhinge's elastic and plastic tangential flexibility matrixes, respectively. The results of experimental studies or numerical analyses of any kind of real hinge zone can be used for determination of $\mathbf{F}_h^p$. In some studies [5-13], associated flow rule has been used for the calculation of $\mathbf{F}_h^p$, as follows:

$$\mathbf{F}_h^p = \frac{\mathbf{n}\mathbf{n}^T}{\mathbf{n}^T\mathbf{K}_p\mathbf{n}}, \tag{12}$$

where, $\mathbf{n}$ is the outward normal unit vector from the yield surface at the point of action and $\mathbf{K}_p$ is a diagonal plastic stiffness matrix from the individual action-deformation relationship for the inner subhinge, as follows:

$$\mathbf{K}_p = \begin{bmatrix} 0 & 0 & 0 \\ 0 & K_{p\nu} & 0 \\ 0 & 0 & K_{pm} \end{bmatrix}. \tag{13}$$

By using Equation 12, flow rule will stay associated and so the plastic deformation vector will always be normal to the yield surface. In the work of Ricles and Popov [12], where shear-flexural interaction was studied, it has been assumed that yield surfaces are rectangular. As shown in Figure 4, by using the associated flow rule, at any point of line AB, $\mathbf{F}_h^p$ is, as follows:

$$\mathbf{F}_h^p = \begin{bmatrix} 0 & 0 & 0 \\ 0 & 0 & 0 \\ 0 & 0 & 1/K_{pm} \end{bmatrix}. \tag{14}$$

And, at any point of line CD, one has:

$$\mathbf{F}_h^p = \begin{bmatrix} 0 & 0 & 0 \\ 0 & 1/K_{p\nu} & 0 \\ 0 & 0 & 0 \end{bmatrix}. \tag{15}$$

So, for the two close points of B and C of which both are very close to the rectangular corner, two quite

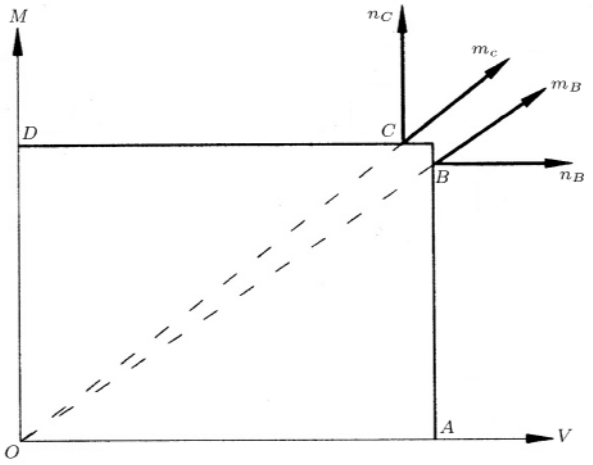

Figure 4. Rectangular yield surface in the shear-flexural space.

different plastic deformations will be resulted. In the present paper, instead of using Equation 12, a different definition for $\mathbf{F}_h^p$ is used, as follows:

$$\mathbf{F}_h^p = \mathbf{m}_V^2 \mathbf{F}_V^p + \mathbf{m}_M^2 \mathbf{F}_M^p, \tag{16}$$

in which $\mathbf{F}_V^p$ and $\mathbf{F}_M^p$ are the flexibility matrixes related to the pure shear and the pure flexural loadings, respectively. m_V and m_M are the components of $\mathbf{m}$ vector in VM space, which is the unit location vector of the action point. As shown in Figure 4, for the points close to the corner, $\mathbf{m}$, $\mathbf{F}_h^p$ and plastic deformations vary smoothly. With this definition, the flow rule will not be associated.

In some non-associated cases, the loading-unloading criteria may fail to differentiate between plastic flow and elastic unloading. To overcome this complexity, the loading-unloading criteria need to be defined more precisely. Suppose the action point lies on a yield surface and the deformation increment is given as $\dot{\mathbf{U}}_h$. First, by using $\mathbf{K}_h = (\mathbf{F}_h^e)^{-1}$, the action rate, $\dot{\mathbf{P}}_h$, is predicted. If $\lambda_1 = \mathbf{n}^T \dot{\mathbf{P}}_h < 0$, the unloading condition exists. For corner points, the unloading condition for both $\mathbf{n}_B$ and $\mathbf{n}_C$ should be satisfied. If $\lambda_1 \geq 0$, by calculating $\mathbf{K}_h = (\mathbf{F}_h^e + \mathbf{F}_h^p)^{-1}$, the new action rate, $\dot{\mathbf{P}}_h$, is obtained. With the new $\dot{\mathbf{P}}_h$, if $\lambda_2 = \mathbf{n}^T \dot{\mathbf{P}}_h > 0$, the plastic loading condition will govern. For corner points, the plastic loading condition needs for only one of $\mathbf{n}_B$ or $\mathbf{n}_C$ to be satisfied. If $\lambda_2 \leq 0$, the stiffness matrix will be adjusted to:

$$\mathbf{K}_h = (\mathbf{F}_h^e + \mathbf{F}_h^p)^{-1} \quad \frac{\lambda_2}{\lambda_1} (\mathbf{F}_h^e)^{-1}. \tag{17}$$

By using the adjusted stiffness and calculating the new action rate, $\dot{\mathbf{P}}_h$, the normality condition, $\mathbf{n}^T \dot{\mathbf{P}}_h = 0$, will result and the natural loading condition will occur. $\mathbf{n}_B$ and $\mathbf{n}_C$ are the unit normal vectors, at points B and C, which are very close to the corner but on two different surfaces (see Figure 4).

YIELD SURFACES

For considering the interaction between shear force and flexure, the multi surface concept in shear-flexural, VM space, is used (see Figure 5). This concept, which was originally defined in stress space [15,16], was adapted with some modifications for the resultant forces space [5-13]. Some of the important aspects and basic assumptions of this concept are, as follows:

1. The yield surfaces are convex;
2. The yield surfaces can be changed in size and translated, but have to be tangential with each other and cannot be intersected;
3. If the action point is internal of the initial yield surface, the behavior will be elastic and, if on each of the surfaces, the behavior will be elastoplastic;
4. In tangency of several yield surfaces, the outer surface properties define the current behavior.

Similarity of yield surfaces is a main assumption in most works, except in some recent studies [12]. The similarity assumption has been used to have parallel directions for the corresponding points on the yield surfaces and, as a result, when the yield surfaces closely approach each other, they will not intersect and, asymptotically, will be tangential to each other. If it is assumed, in shear-flexural space, that yield surface, i, is similar to yield surface, j, then, one will have:

$$\frac{V_{yi}}{V_{yj}} = \frac{M_{yi}}{M_{yj}}, \tag{18}$$

where, V_{yi}, V_{yj}, M_{yi} and M_{yj} are the points on i and j yield surfaces for the pure shear and bending loading (see Figure 5). This is not a realistic assumption, generally.

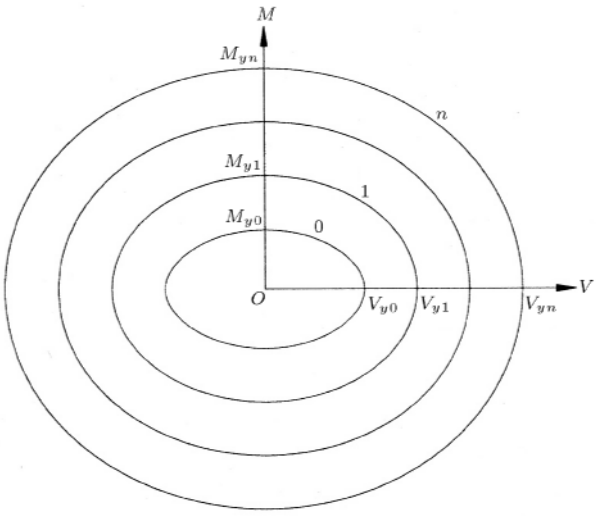

Figure 5. Typical yield surfaces in the multi-surfaces model.

Ricles and Popov [12] overcame this problem by choosing a rectangular yield surface with different ratios of length to width, but, it is noted that, with the use of rectangular yield surfaces, the interaction of shear-bending is ignored, practically. In the present research, by considering piecewise dissimilar yield surfaces, as shown in Figure 6, the above shortcoming is resolved and shear-flexural interaction is considered, more realistically. The yield surfaces may have polygonal shapes. For preventing the intersection of yield surfaces, the corresponding sides of all yield surfaces should be parallel to each other and the length of any side of any yield surface should be smaller than the length of the corresponding side of the outer yield surface.

HARDENING RULE

The hardening rule defines the manner by which the yield surface changes. For all of the surfaces, translation (kinematic hardening) and, also, change in size (isotropic hardening), are permitted, except for the last yield surface. The last yield surface is assumed to have a change in size, only because the final plastic capacity of a section is constant. The same as in some recent works [5-13], the element formulation is based on combined kinematic and isotropic hardening for the shear force, and only kinematic hardening for flexure. On this basis, the ith yield function is written, as follows:

$$\phi_i(\mathbf{P}_h \quad \boldsymbol{\alpha}_i, H_i) = 0, \tag{19}$$

where, $\mathbf{P}_h$ is the action vector of the subhinge. $\boldsymbol{\alpha}_i$ and H_i are the ith yield function center and its expansion parameter, respectively.

For developing the shear isotropic hardening, the following is adopted [17]:

$$V_{yie} = H_i V_{yi}, \tag{20}$$

where, V_{yi} and V_{yie} are the initial and developed values of the shear force at ith yielding, respectively. H_i is written as:

$$H_i = 1 + C_1[1 \quad C_2 \exp(\quad v_{hp})], \tag{21}$$

where:

$$v_{hp} = \int |dv_h^p|, \tag{22}$$

and C_1 and C_2 are material constants.

Various kinematic hardening rules were used in most recent works [7,12,13]. In this paper, a new kinematic hardening rule is introduced. As seen in Figure 7, it is assumed that the action location is on the ith yield surface and plastic loading is occurring. The rate of the ith yield surface translation, $\dot{\alpha}_i$, is assumed as being:

$$\dot{\alpha}_i = (\mathbf{P}_{hi+1} \quad \mathbf{P}_{hi})\dot{\boldsymbol{\mu}}, \tag{23}$$

where, $\mathbf{P}_{hi+1}$ is the intersection point between the direction of the action rate, $\dot{\mathbf{P}}_h$, and the $(i+1)$th yield surface, and $\mathbf{P}_{hi}$ is the conjugate point of $\mathbf{P}_{hi+1}$ on the ith yield surface. By this definition, when the action point, $\mathbf{P}_h$, approaches closer to the $(i+1)$th yield surface, the ith yield surface moves, such that the two points on the ith yield surface, $\mathbf{P}_{hi}$ and $\mathbf{P}_h$, approach closer to each other and coincide with $\mathbf{P}_{hi+1}$, asymptotically. It shows that the inner moving yield surface may be tangential to the outer yield surface at the contact point and they never intersect.

To calculate $\dot{\boldsymbol{\mu}}$, the plastic loading condition is used:

$$\dot{\phi}_i = 0. \tag{24}$$

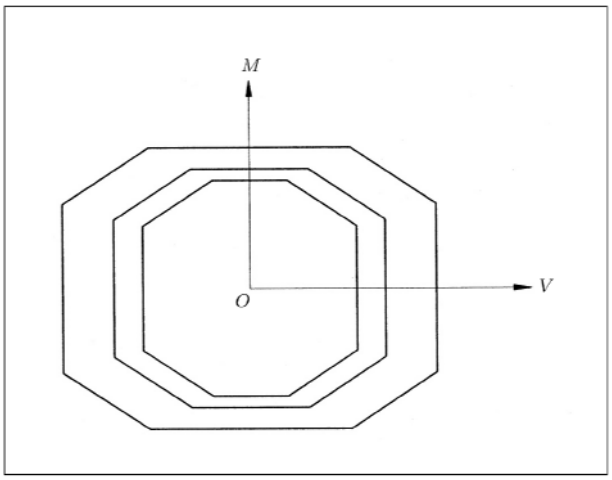

Figure 6. Typical piecewise dissimilar yield surfaces used for the mixed hinge element.

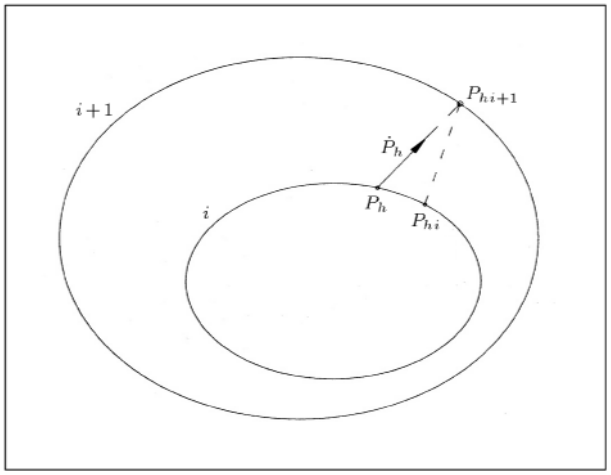

Figure 7. Action point and corresponding points on two adjacent yield surfaces.

Hence:

$$\frac{\partial \phi_i}{\partial \mathbf{P}_h}\dot{\mathbf{P}}_h + \frac{\partial \phi_i}{\partial \boldsymbol{\alpha}_i}\dot{\boldsymbol{\alpha}}_i + \frac{\partial \phi_i}{\partial H_i}\dot{H}_i = 0. \tag{25}$$

And, since one has:

$$\frac{\partial \phi_i}{\partial \mathbf{P}_h} = \frac{\partial \phi_i}{\partial \boldsymbol{\alpha}_i}, \tag{26}$$

so, Equation 25 can be written as:

$$\frac{\partial \phi_i}{\partial \mathbf{P}_h}\dot{\mathbf{P}}_h = \frac{\partial \phi_i}{\partial \mathbf{P}_h}\dot{\boldsymbol{\alpha}}_i \quad \frac{\partial \phi_i}{\partial H_i}\dot{H}_i. \tag{27}$$

After pre-multiplying both sides of Equation 23 by $\frac{\partial \phi_i}{\partial \mathbf{P}_h}$, one reaches the following:

$$\frac{\partial \phi_i}{\partial \mathbf{P}_h}\dot{\boldsymbol{\alpha}}_i = \frac{\partial \phi_i}{\partial \mathbf{P}_h}(\mathbf{P}_{hi+1} \quad \mathbf{P}_{hi})\dot{\boldsymbol{\mu}}. \tag{28}$$

Comparing the last two equations results in the following:

$$\frac{\partial \phi_i}{\partial \mathbf{P}_h}\dot{\mathbf{P}}_h = \frac{\partial \phi_i}{\partial \mathbf{P}_h}(\mathbf{P}_{hi+1} \quad \mathbf{P}_{hi})\dot{\mu} \quad \frac{\partial \phi_i}{\partial H_i}\dot{H}_i, \tag{29}$$

or:

$$\dot{\mu} = \frac{\frac{\partial \phi_i}{\partial \mathbf{P}_h}\dot{\mathbf{P}}_h + \frac{\partial \phi_i}{\partial H_i}\dot{H}_i}{\frac{\partial \phi_i}{\partial \mathbf{P}_h}(\mathbf{P}_{hi+1} \quad \mathbf{P}_{hi})}. \tag{30}$$

By substituting Equation 30 in Equation 23, $\dot{\alpha}_i$ can be determined, as follows:

$$\dot{\boldsymbol{\alpha}}_i = \frac{\frac{\partial \phi_i}{\partial \mathbf{P}_h}\dot{\mathbf{P}}_h + \frac{\partial \phi_i}{\partial H_i}\dot{H}_i}{\frac{\partial \phi_i}{\partial \mathbf{P}_h}(\mathbf{P}_{hi+1} \quad \mathbf{P}_{hi})}(\mathbf{P}_{hi+1} \quad \mathbf{P}_{hi}), \tag{31}$$

$\dot{\alpha}_i$ is the parameter of the translation criteria for the ith yield surface, due to loading.

COMPARISON WITH SOME EXISTING TEST RESULTS

In this part, the capability of the proposed mixed hinge element for link beams in EBFs is investigated. For the first example, the medium link beam tested by Kasai and Popov [18] and analyzed by Ricles and Popov [12], is investigated. The link element consists of a W8 × 10 link beam, with a length of $L = 368$ mm. The shear capacity of the element's section is $V_p = 205.5$ kN and the flexural capacity is $M_p = 56.3$ kN-m. The element was subjected to cyclically symmetric deformations. Regarding the end conditions of the element in the laboratory, the stiffness of the right end was more than that of the left. So, shear and flexural yielding in the element has been started from the right end with a redistribution of flexural end moments during yielding. For modeling by the mixed hinge element, the location of the inner subhinge is assumed to be at the right end ($L_i = L$, $L_j = 0$). For C_1 and C_2 parameters of Equation 21, based on regression analysis, the values of 0.8 and 10 were proposed, respectively [17]. In the present study, with some trial, the values of 0.35 and 15 are used for C_1 and C_2, respectively. The yield surfaces used for this example have been shown in Figure 8. These shapes, chosen for yield surface, are based on a set of experimental results presented by Kasai and Popov [18]. The flexibility matrix for the inner subhinge is assumed to be as follows:

$$\mathbf{F}_h = \begin{bmatrix} \frac{L}{EA} & 0 & 0 \\ 0 & \frac{1}{k_1}\frac{L^3}{3EI} + \frac{1}{k_2}\frac{L}{GA_s} & \frac{1}{k_3}\frac{L^2}{2EI} \\ 0 & \frac{1}{k_3}\frac{L^2}{2EI} & \frac{1}{k_4}\frac{L}{EI} \end{bmatrix}, \tag{32}$$

where, E and G are Young's modulus and the modulus of rigidity of the section material and A, I and A_s are area, moment of inertia and shear area of the link section, respectively. k_1, k_2, k_3 and k_4 in the above matrix, are the constants which represent the stiffness ratio between each two yield surfaces for two conditions of pure shear and bending loading. In the mentioned works [12,17], the stiffness ratios between each two yield points in the shear-deflection or flexural-rotation diagrams, were assumed to be 0.03, 0.015 and 0.002, as seen in Figure 9. In the present work, regarding the difference between the failure modes of pure shear and flexural loading and with some trial, the k_1, k_2, k_3 and k_4 ratios have been selected, as shown in Tables 1 and 2. The experimental [18] and analytical results are compared in Figure 10, where, horizontal axes (Dis.) indicate the relative shear deformation between the two ends of the link beam. As shown, the mixed hinge

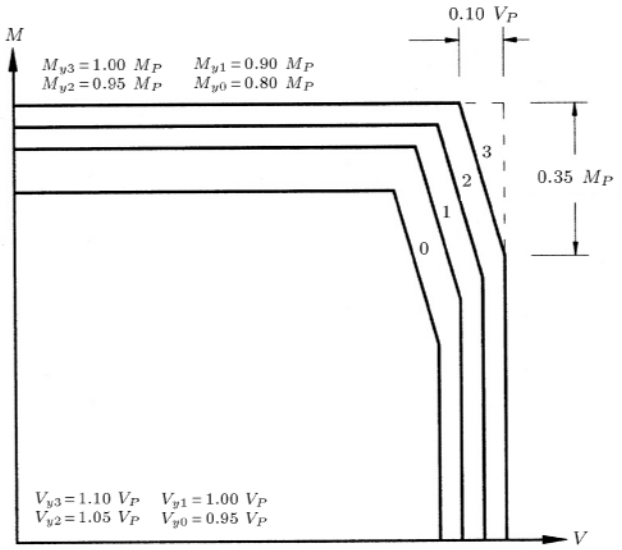

Figure 8. Yield surfaces of mixed hinge element used for the link elements.

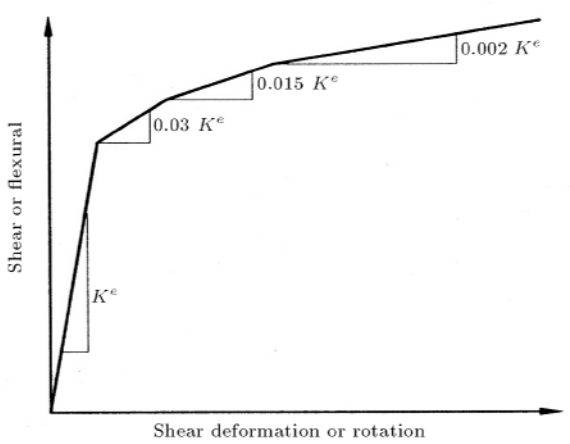

Figure 9. Typical multilinear load-deformation relation.

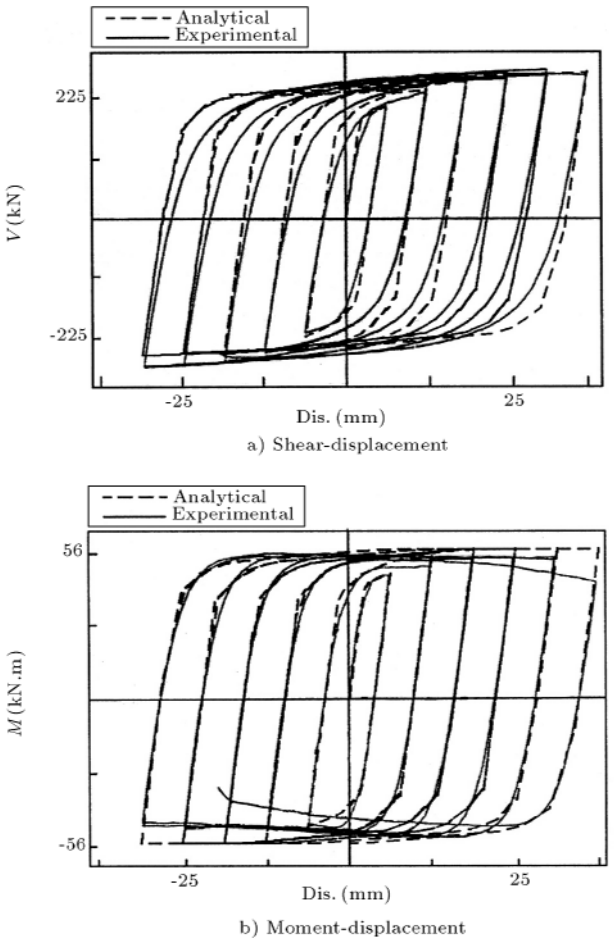

Figure 10. Experimental measurements and analytical results of the medium length link beam.

results are in good agreement with the test results. The manner of expansion and translation of yield surfaces in the mixed hinge are shown in Figure 11. As seen, yielding reached the shear-flexural interaction zone, firstly. Then, the behavior of the element was controlled by the flexural capacity of the element.

For the second example, the shortest link element

Table 1. Constants of flexibility matrixes for pure shear loading of the link beams.

Between Yield Surfaces	k_1	k_2	k_3	k_4
0 and 1	0.060	0.060	0.060	0.060
1 and 2	0.030	0.030	0.030	0.030
2 and 3	0.010	0.010	0.010	0.010

Table 2. Constants of flexibility matrixes for pure flexural loading of the link beams.

Between Yield Surfaces	k_1	k_2	k_3	k_4
0 and 1	0.030	0.300	0.030	0.030
1 and 2	0.015	0.150	0.015	0.015
2 and 3	0.002	0.020	0.002	0.002

tested by Kasai and Popov [18] is investigated. The length of this element is $L = 292$ mm and its other configurations are the same as in the foregoing example. The failure mode of this element is different and shear yielding controlled the behavior of the element. All of the parameters used for modeling by the mixed hinge element are the same as in the foregoing example. The experimental [18] and analytical results are compared in Figure 12, which shows that the analytical and experimental results are in excellent agreement.

Although the length and the failure modes of the two previous examples are different, the developed mixed hinge element explained the behavior of both links, with acceptable accuracy.

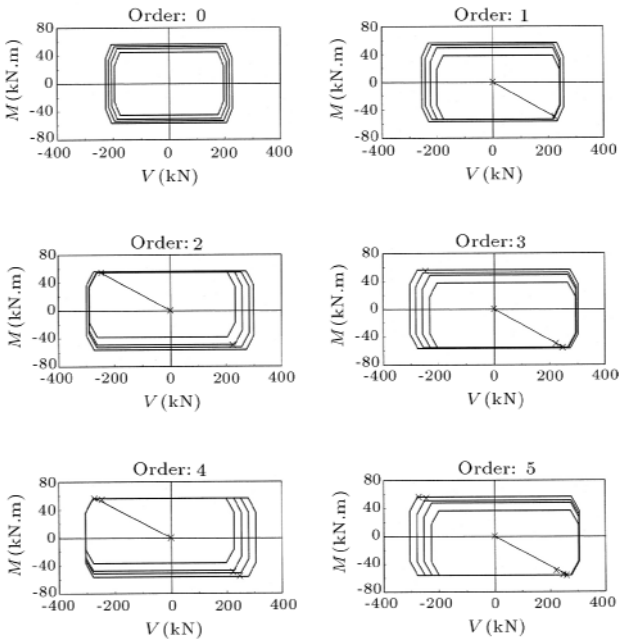

Figure 11. The yield surfaces expansion and translation sequences of the medium length link beam.

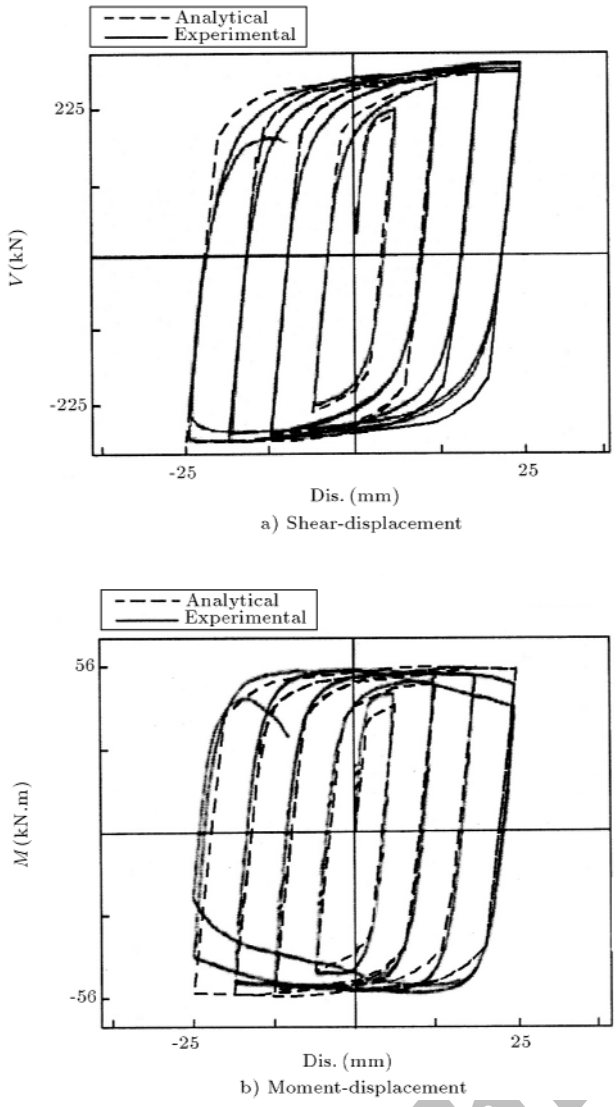

Figure 12. Experimental measurements and analytical results of the short length link beam.

APPLICATION OF THE MODEL ON REDUCED WEB SECTION BEAMS

Reduced web section beams in shear-yielding moment-resistant steel frames have been investigated recently [19]. These beams are used in steel frames for earthquake energy dissipation by shear yielding of their reduced webs. In this part, the modeling of the reduced web zones of these beams is examined by using the mixed VM hinge element. Three reduced web section beams, with equal sections but different span lengths, as shown in Figure 13, are investigated. The beams consist of W21 $\times$ 68 (A = 13131 mm^2, I = 625770000 mm^4 and A_s = 5900 mm^2), with span lengths of 2520, 3780 and 6720 mm and two circular holes at the ends. The diameter of each hole is 420 mm and its center is located 630 mm from the closer end. Multi-linear kinematic hardening plasticity is assumed

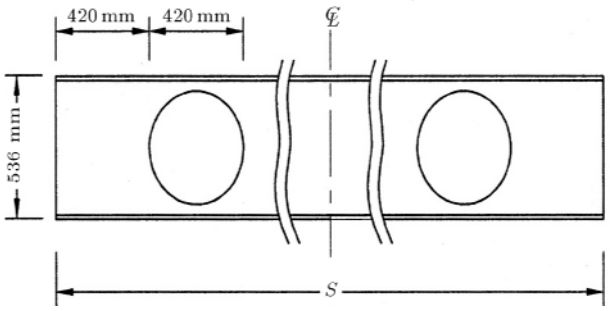

Figure 13. Geometrical configuration of the reduced web section beams.

for the material of the beams, with F_y = 360 MPa, F_u = 500 MPa, E = 200 GPa, $H = 0.005E$ = 1 GPa and ν = 0.3. Where F_y and F_u are the yield and ultimate stress, E and H are the initial and post yield modulus of elasticity and ν is the Poisson ratio. All of the beams are subjected to cyclically symmetric relative displacements between two ends, as shown in Figure 14. The analysis is done statically and rotational freedom at both ends is prevented. The beams are analyzed with a finite element program at the first stage. In these analyses, eight-node solid elements with nonlinear material behavior, in accordance with von-Mises criteria, are used. Regarding beam symmetry, half the beams are modeled. The maximum element dimension is 50 mm. The beams are reanalyzed by using the proposed model at the second stage. In these analyses the two mixed hinge elements, with a length of L = 1260 mm, are used at both ends of the beams. Location of the subhinge is assumed to be in the middle of the hinge element ($L_i = L_j$ = 630 mm), coincident to the center of the hole, as shown in Figure 15. The hinge element, analyzed between the two for pure shear and pure flexural, separately, by using the finite element method and the mixed hinge element property, is obtained. The resulted yield surfaces are shown in Figure 16. The inner subhinge flexibility matrixes in

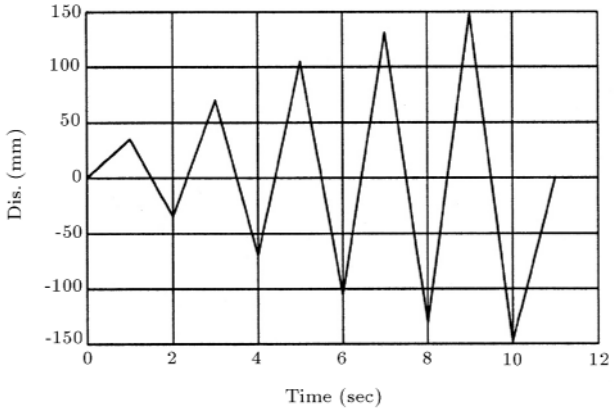

Figure 14. Displacement history applied to the reduced web section beams.

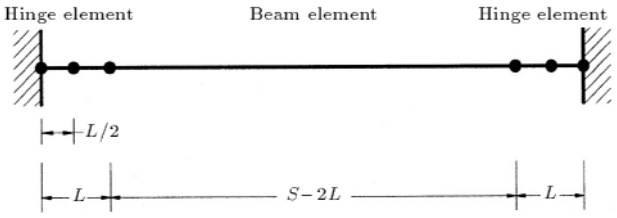

Figure 15. Modeling of the reduced web section beams with a beam and two mixed hinge elements.

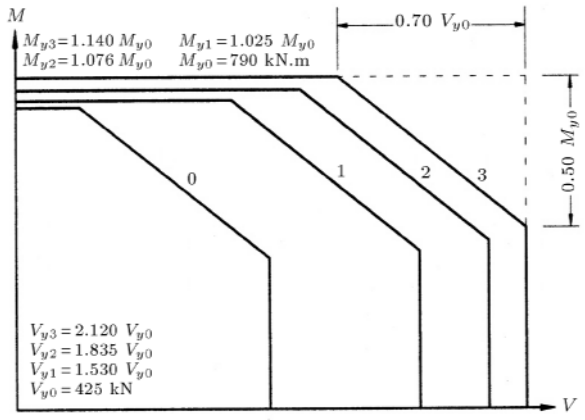

Figure 16. Yield surfaces used in the mixed hinge element for modeling of the reduced web section beams.

consecutive yield surfaces are assumed to be, as follows:

$$\mathbf{F}_h = \begin{bmatrix} 1 & 0 & 0 \\ 0 & 1 & L/2 \\ 0 & 0 & 1 \end{bmatrix} \begin{bmatrix} \frac{1}{r_0}\frac{L}{EA} & 0 & 0 \\ 0 & \frac{1}{k_1}\frac{1}{r_1}\frac{L^3}{3EI} + \frac{1}{k_2}\frac{1}{r_2}\frac{L}{GA_s} & \frac{1}{k_3}\frac{1}{r_3}\frac{L^2}{2EI} \\ 0 & \frac{1}{k_3}\frac{1}{r_3}\frac{L^2}{2EI} & \frac{1}{k_4}\frac{1}{r_4}\frac{L}{EI} \end{bmatrix} \begin{bmatrix} 1 & 0 & 0 \\ 0 & 1 & 0 \\ 0 & L/2 & 1 \end{bmatrix} \quad (33)$$

The k_1, k_2, k_3 and k_4 hardening coefficients are selected, as seen in Table 3 and equivalent effective stiffness factors, obtained from the finite element analysis, are $r_0 = 0.883$, $r_1 = 0.983$, $r_2 = 0.592$, $r_3 = 0.977$ and $r_4 = 0.977$. Since isotropic hardening is ignored, then, one has $C_1 = C_2 = 0$ (Equation 21). The finite element model and the mixed hinge element results are compared in Figures 17 to 19. As shown, the mixed hinge results are in fairly suitable agreement with the finite element results. The manner of translation of yield surfaces in the mixed hinge modeling is shown in Figures 20 to 22. In these figures, shear and flexural

Table 3. Constants of flexibility matrixes for pure shear and pure flexural loadings of the reduced web section beams.

Between Yield Surfaces	Pure Shear	Pure Flexural
0 and 1	0.300	0.333
1 and 2	0.038	0.033
2 and 3	0.005	0.004

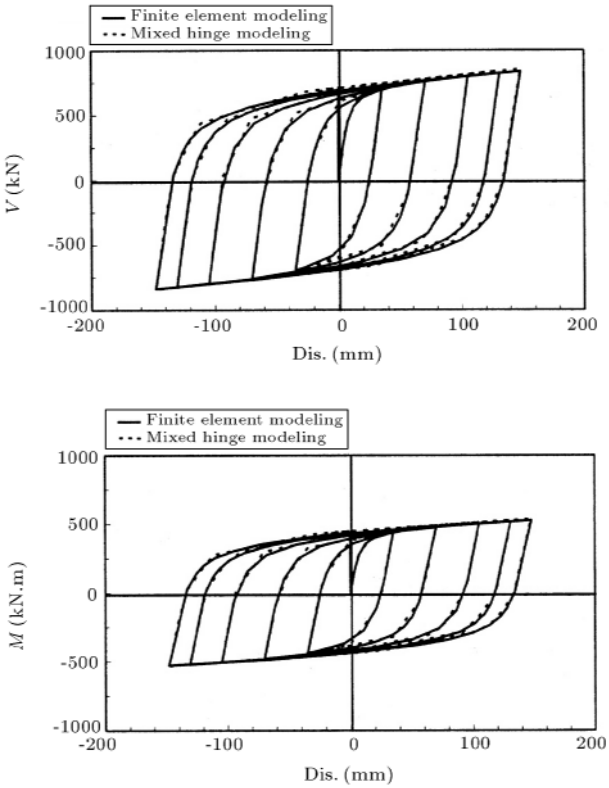

Figure 17. The comparison between finite element analysis and mixed hinge element results of the reduced web section beam with span of $S = 2520$ mm.

moment are the internal forces in the location of the inner subhinge (hole center), and displacement is the relative transverse displacements between the two ends of the beam. As shown in the first model, the shear capacity is governed and, in the third model, the flexural capacity controls the behavior of the beam. However, in the second beam, the action point is located at the shear-flexural interaction zone. Although, in the three beams, the failure modes are different, the results of the presented mixed hinge element modeling have good accuracy.

It is observed that using an octahedral yield surface instead of a rectangular yield surface is more efficient, especially for the reduced web section beam with a medium span ($S = 3780$ mm), where the action point is located on the oblique line of the octahedral yield surface (see Figure 21). In Figure 23, the results

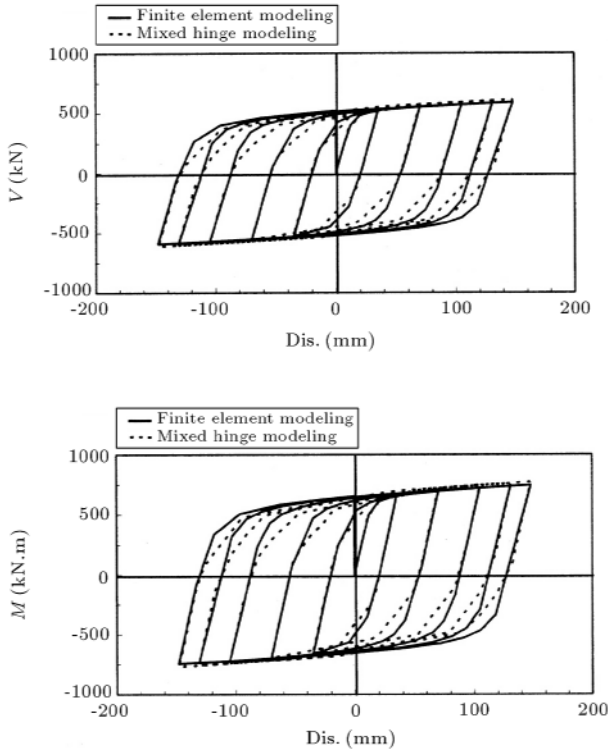

Figure 18. The comparison between finite element analysis and mixed hinge element results of the reduced web section beam with span of $S = 3780$ mm.

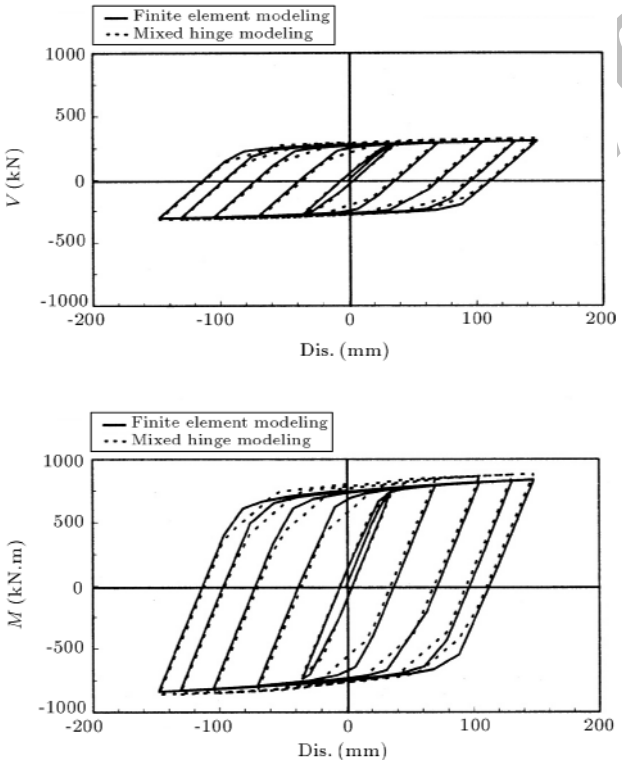

Figure 19. Shear-displacement and moment-displacement comparison between finite element analysis and mixed hinge element results of the reduced web section beam with length $S = 6720$ mm.

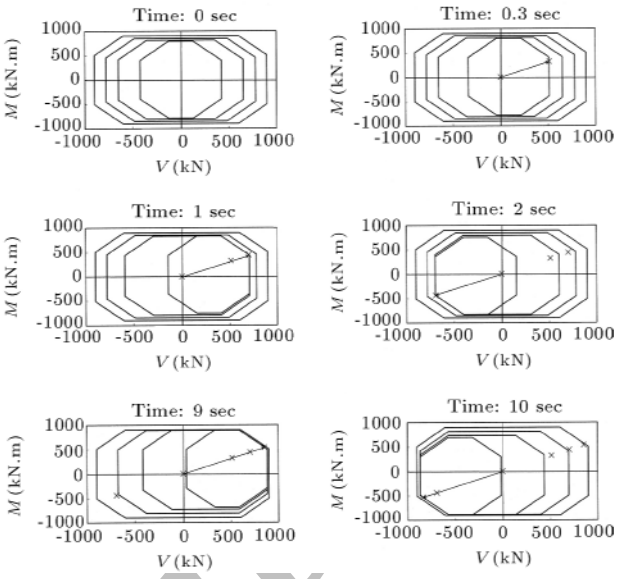

Figure 20. Translation history of yield surfaces for the mixed hinge element of the reduced web section beam with span of $S = 2520$ mm.

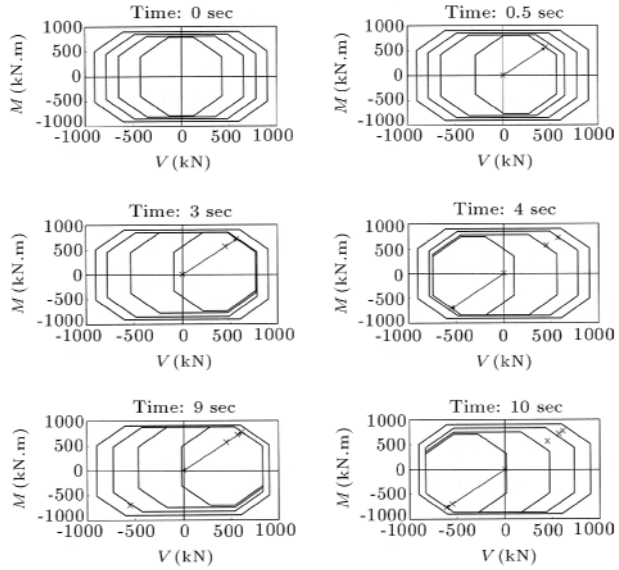

Figure 21. Translation history of yield surfaces for the mixed hinge element of the reduced web section beam with span of $S = 3780$ mm.

of the reduced web section beam with medium span, using octahedral and rectangular yield surfaces, are compared with the finite element result. As seen, the octahedral yield surface model result is more realistic and closer to the finite element result.

The requirement of using the proposed element, considering shear-flexural interaction, is clarified in Figure 24. In this figure, the flexural moment at the inner subhinge, the center of the web hole, is presented against the monotonic rotation of the inner subhinge and pure flexural loading is compared with shear-

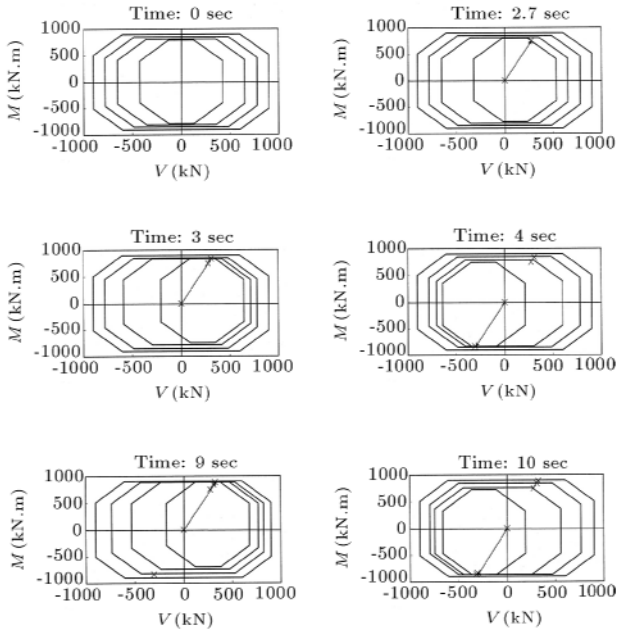

Figure 22. Translation history of yield surfaces for the mixed hinge element of the reduced web section beam with span of $S = 6720$ mm.

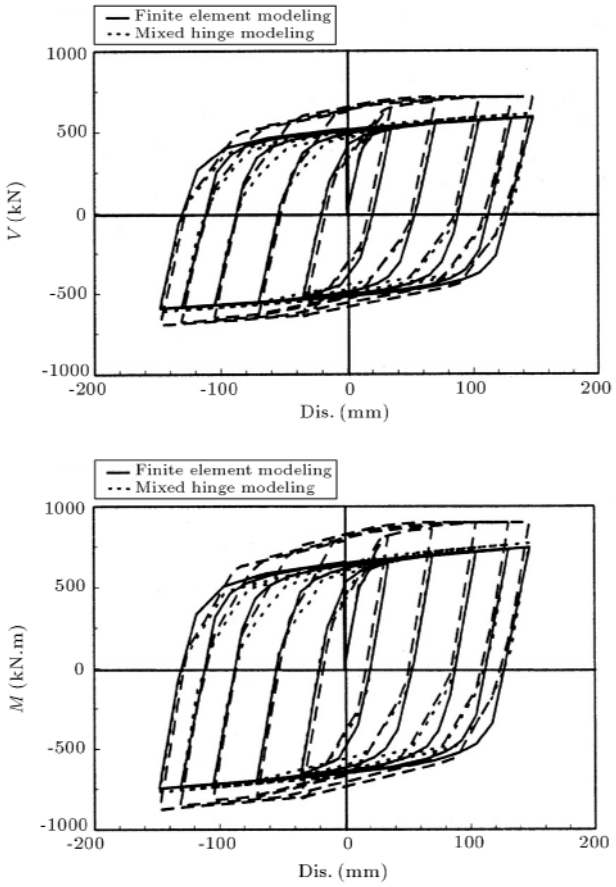

Figure 23. Comparison of the finite element analysis (solid line) with the mixed hinge element analyses using the octahedral yield surfaces (dot line) and the rectangular yield surfaces (dashed line).

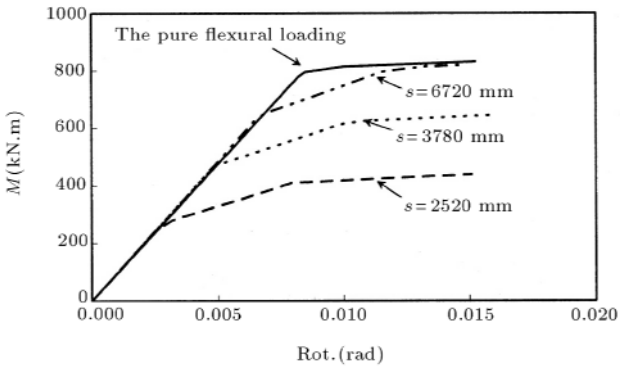

Figure 24. Shear force effect on moment-rotation relationship for the three reduced web section beams with different spans.

flexural loading in three reduced web section beams. It is observed that the pure flexural loading result is very different from the other cases and the effect of shear force on the reduction of the flexural capacity of the element increases by reducing the beam span length.

CONCLUSIONS

In this paper, a new shear-flexural mixed hinge element was developed for consideration of the interaction between internal forces, for two dimensional frame analyses. The hinge element could have a nonzero length to model plastic zones in the beams. A multi-surfaces concept was used for the modeling of the mixed hinge element, by proposing dissimilar yield surfaces and suggesting off-diagonal members in flexibility matrixes. A new procedure for plastic loading on yield surfaces suggested insuring a smooth variation of the hinge flexibility matrix. Also, a new kinematic hardening rule was introduced to prevent any intersection of the dissimilar yield surfaces. The mixed hinge element was examined for some link beams in EBFs and reduced web section beams in shear-yielding moment-resistant steel frames. The proposed analytical results were compared with existing experimental results (for link beams) and finite element results (for reduced web section beams) and close agreements were observed.

REFERENCES

1. Horne, M.R. and Morris, L.J., *Plastic Design of Low-Rise Frames*, Collins, London, Constrado Monographs (1981).
2. Chen, W.F. and Lui, E.M., *Stability Design of Steel Frames*, Boca Raton, Fl: CRC Press (1991).
3. Mazzolani, F.M. and Piluso, V., *Theory and Design of Seismic Resistant Steel Frames*, London, E & FN Spon (1996).
4. Jirasek, M. and Bazant, Z.P., *Inelastic Analysis of*

Structures, John Wiley & Sons, LTD, New York, USA (2002).

5. Powell, G.H. and Chen, P.F.S. "3D beam-column element with generalized plastic hinges", *ASCE J. of Eng. Mech.*, **112**(7), pp 627-641 (1986).
6. Krenk, S., Vissing, S. and Vissing-J., C. "A finite step updating method for elastoplastic analysis of frames", *ASCE J. of Eng. Mech.*, **119**(12), pp 2478-2495 (1993).
7. Kim, K.D. and Engelhardt, M.D. "Beam-column element for nonlinear seismic analysis of steel frames", *ASCE J. of Struct. Eng.*, **126**(8), pp 916-925 (2000).
8. Liew, J.Y.R. and Tang, L.K. "Advanced plastic hinge analysis for the design of tubular space frames", *Eng. Struct.*, **22**(7), pp 769-783 (2000).
9. Liew, J.Y.R., Chen, W.F. and Chen, H. "Advanced inelastic analysis of frame", *J. of Construct. Steel Res.*, **55**(3), pp 245-265 (2000).
10. Liew, J.Y.R., Chen, H., Shanmugam, N.E. and Chen, W.F. "Improved nonlinear plastic hinge analysis of space frame structures", *Eng. Struct.*, **22**(10), pp 1324-1328 (2000).
11. El-Tawil, S. and Deierlein, G.G. "Stress-resultant plasticity for frame structures", *ASCE J. of Eng. Mech.*, **124**(12), pp 1360-1370 (1998).
12. Ricles, J.M. and Popov, E.P. "Inelastic link element for EBF seismic analysis", *ASCE J. of Struct. Eng.*, **120**(2), pp 441-463 (1994).
13. Ricles, J.M., Yang, Y.S. and Priestley, M.J.N. "Modeling nonductile R/C columns for seismic analysis of bridges", *ASCE J. of Struct. Eng.*, **124**(4), pp 415-424 (1995).
14. Saritas, A. and Filippou, F.C. "Modeling of shear-yielding members for seismic energy dissipation", *13th World Conference on Earthquake Engineering*, Paper No. 1799 (2004).
15. Khan, A.S. and Huang, S., *Continuum Theory of Plasticity*, John Wiley & Sons. Inc., New York, USA (1995).
16. Mroz, Z. "An attempt to describe the behavior of metals under cyclic loads using a more general workhardening model", *Acta Mechanica*, **7**(2-3), pp 199-212 (1969).
17. Ramadan, T. and Ghobarah, A. "Analytical model for shear link behavior", *ASCE J. of Struct. Eng.*, **121**(11), pp 1574-1580 (1995).
18. Kasai, K.S.M. and Popov, E.P. "General behavior WF steel shear link beams", *ASCE J. of Struct. Eng.*, **12**(2), pp 362-382 (1986).
19. Halterman, A. and Aschheim, M. "Analytical studies of shear-yielding moment-resistant steel frames", *12th World Conference on Earthquake Engineering*, Paper No. 1544 (2000).